

# Local kinetic energy budget of high-frequency and intermediate-frequency eddies: winter climatology and interannual variability

Tianyu Jiang · Yi Deng · Wenhong Li

Received: 6 May 2012 / Accepted: 28 January 2013 / Published online: 14 February 2013  
© Springer-Verlag Berlin Heidelberg 2013

**Abstract** The local budget of eddy kinetic energy (EKE) for both high-frequency (HF, 2–6 days) and intermediate-frequency (IF, 7–29 days) eddies are evaluated for Northern Hemisphere boreal winter using the 31-year (1979/80–2010/11) NCEP-DOE reanalysis. A new form of EKE equation is used to isolate the kinetic energy generation/destruction due to interactions among eddies of different timescales. The main source of HF EKE is baroclinic conversion that is concentrated in the mid-lower troposphere. Barotropic conversion mainly damps HF EKE and shows positive contributions to IF EKE on the northern flank of the winter-mean tropospheric jet. Interaction between HF and IF eddies acts as a sink for HF EKE and a main source for IF EKE, especially over the eastern ocean basins, confirming the substantial role of synoptic-scale transients in the development of IF phenomena such as atmospheric blocking. Large interannual variability is found for various EKE budget terms. The HF EKE response to El Niño is characterized by a dipole (tri-pole) anomaly over the North Pacific (North Atlantic). Baroclinic conversion is the main driver of the observed changes in HF EKE while barotropic conversion, interaction between HF and IF eddies, and energy flux convergence all play non-negligible roles in determining the final meridional structure of the HF EKE anomalies. Associated with El Niño, IF EKE generally decreases over the North Pacific and increases over the North Atlantic, which mainly result

from changes in baroclinic conversion and EKE conversion due to eddy–eddy interactions. The latter is dominated by interaction between IF and LF (low-frequency, 30–90 days) eddies over the North Pacific, and by interactions between HF and IF eddies, and between IF and LF eddies over the North Atlantic.

**Keywords** High-frequency eddies · Intermediate-frequency eddies · Kinetic energy · Eddy-eddy interaction

## 1 Introduction

Energetics is a critical component of our understanding of the general circulation of the atmosphere (Peixoto and Oort 1992). Following the pioneering work of Lorenz (1955), numerous studies have examined extensively the magnitude and direction of energy exchange among various forms of atmospheric energy of the mean flow and of eddies of different temporal and spatial scales (e.g., Wiin-Nielsen 1962; Oort 1964; Plumb 1983; Sheng and Hayashi 1990a, b). These studies reveal the conversion and cycling of atmospheric energy on a global, integrated sense and have taken approaches similar to the one used to construct the original Lorenz energy cycle (Lorenz 1955). Local energetics, on the other hand, emphasizes in addition the spatial structure of energy conversions. Mak and Cai (1989) and Cai and Mak (1990) diagnosed local energetics to understand modal and nonmodal instability of a barotropic jet and to delineate the dynamics of regional cyclogenesis in a two-layer channel model. Orlanski and Katzfey (1991) employed the concept of local energetics to explain the lifecycle of a Southern Hemisphere cyclone and highlighted the importance of the divergence of ageostrophic geopotential flux in the evolution of the cyclone.

T. Jiang (✉) · Y. Deng  
School of Earth and Atmospheric Sciences, Georgia Institute of Technology, 311 Ferst Drive, Atlanta, GA 30332-0340, USA  
e-mail: jiangty@gatech.edu

W. Li  
Earth and Ocean Sciences, Nicholas School, Duke University, Durham, NC, USA

Deng and Mak (2005, 2006) and Mak and Deng (2007) adopted local energetics analysis to quantify the role of “barotropic-governor” effect in contributing to the mid-winter suppression of the North Pacific storm track (e.g., Nakamura 1992).

The interaction, and thus energy exchange among disturbances of different scales in a broad sense determines the main characteristics of internal atmospheric variability and the associated climate phenomena across synoptic to intraseasonal timescales (e.g., Dole 2008). The dynamical implications of eddies with timescales beyond a week have been long recognized (e.g., Blackmon et al. 1984a, b). These so-called intermediate-frequency (IF) eddies usually manifest themselves as a blocking, a persistent anomaly or a specific teleconnection pattern, and are always coupled with variability in the activity of synoptic eddies (e.g., Dole and Gordon 1983; Trenberth 1986; Lau 1988; Nakamura and Wallace 1990; Dole and Black 1990; Black 1997; Holton 2004). Namias (1947) made the first attempt to identify the role of synoptic eddies in blocking events that occurred during the winter of 1946/1947. More recent studies further confirmed that the onset and maintenance of blocking events are associated with nonlinear interactions between large scale, low frequency waves and synoptic waves (Shutts 1983; Mullen 1987; Nakamura et al. 1997; Tyrlis and Hoskins 2008). However, to achieve a reliable simulation of blocking events in climate model is still a challenging task (Scaife et al. 2010). Although part of the difficulty is attributed to the limitation of the model resolution (Matsueda et al. 2009), most of the biases in simulating blocking events likely result from an unsatisfactory representation of various nonlinear processes including scale-interactions (Doblas-Reyes et al. 2002; Barriopedro et al. 2010).

The interaction between synoptic, high-frequency (HF) eddies and IF eddies and the associated nonlinear energy conversion have been an important topic in many studies of local energetics. For example, Mak (1991) applied local energetics analysis to a blocking event and proved that the mechanism of “synoptic-eddy-straining” is particularly important for the development of the blocking. Sheng and Derome (1991) calculated in frequency domain the energy conversions among available potential energy (APE) and kinetic energy (KE) of seasonal mean flow, fast transients (eddies with periods shorter than 10 days) and slow transients (eddies with periods longer than 10 days), and showed that slow transients are maintained by both baroclinic and nonlinear conversion when hemispherically-integrated quantities are considered. Most recently, Deng and Jiang (2011) analyzed the local kinetic energy budget of synoptic-scale and low-frequency transients to understand the interaction between the North Pacific storm track and tropical intraseasonal variability in boreal winter. With

a similar approach, Hsu et al. (2010) examined the impact of tropical intraseasonal oscillation on the summertime eddy kinetic energy (EKE) budget over the western Pacific.

In Deng and Jiang (2011), a new form of the synoptic eddy kinetic energy equation was derived where energy conversions by Reynolds stresses were separated into energy generation due to interactions between eddy and time-mean flow and due to eddy–eddy interactions. Given the effects of IF eddies on extratropical climate variability and their close tie with HF eddies that bring day-to-day weather variability, here we extend the analysis in Deng and Jiang (2011) to further examine the role of cross-frequency, eddy–eddy interactions in the local, climatological EKE budget. This study is in part motivated by the potential applicability of this method to climate model evaluations that aim to identify sources of biases in the simulations of IF phenomena such as atmospheric blocking. Specific goals of this analysis are to (1) construct the local, climatological kinetic energy budget for HF and IF eddies; (2) understand regional variations in various energy conversion terms, and (3) quantify the winter interannual variability in local energy conversion and in particular, illustrate the response of various energy conversion processes to the tropical Pacific SST forcing. Following this introduction, in Sect. 2 we describe the HF/IF EKE equations, data, and analysis technique used in the study. The 3-dimensional (3D) winter climatology of the EKE budget terms is examined in detail in Sect. 3, together with a discussion of the interannual variability in the EKE budget. As an essential component of the interannual variability, the response of individual energy conversion processes to ENSO (El Niño–Southern Oscillation) forcing is also discussed. Section 4 gives some concluding remarks.

## 2 Data and methods

Following Deng and Jiang (2011), we derive the EKE equation starting from the momentum equation of transient eddies

$$\frac{\partial \bar{V}_T}{\partial t} = -\bar{V}_{3M} \times \nabla_3 \bar{V}_T - \bar{V}_{3T} \times \nabla_3 \bar{V}_M - \bar{V}_{3T} \times \nabla_3 \bar{V}_T - \bar{V}_{3T} \times \nabla_3 \bar{V}_T - \nabla \Phi_T - f\bar{k} \times \bar{V}_T + \bar{F}_{rT} \quad (1)$$

where  $\bar{V}$  and  $\bar{V}_3$  stand for horizontal and three-dimensional wind vector, respectively;  $\Phi$  is geopotential;  $f$  is Coriolis parameter, and  $\bar{F}_r$  is the viscous force. Subscripts “ $T$ ”, and “ $M$ ” in (1) represent the transient eddy and time-mean component of the flow, respectively. The overbar here stands for time mean. The transient eddy component here,

obtained as departure from the seasonal mean in the calculation, is further broken down into 3 frequency bands: high frequency (HF, 2–6 days), intermediate frequency (IF, 7–29 days) and low frequency (LF, 30–90 days). Note that the definitions of the frequency bands adopted here are slightly different compared to those used in Deng and Jiang (2011) due to the use of a “sharper” bandpass filter. The results to be presented are not sensitive to the small changes in the definition of eddies. Applying an HF bandpass filter to (1), we obtain the momentum equation for HF eddies as follows,

$$\frac{\partial \bar{V}_H}{\partial t} = -\bar{V}_{3M} \times \nabla_3 \bar{V}_H - \bar{V}_{3H} \times \nabla_3 \bar{V}_M - \overline{\bar{V}_{3H} \times \nabla_3 \bar{V}_H}^H - \nabla \Phi_H - \bar{f}k \times \bar{V}_H + \bar{F}_{rH} \tag{2}$$

where subscript “H” indicates the HF component of the total eddy field and overbar with superscript “H” denotes the HF bandpass filtering.

Taking the dot product of (2) with  $\bar{V}_H$ , utilizing hydrostatic balance and the continuity equation in pressure coordinates, we obtain the following HF EKE equation,

$$\frac{\partial K_H}{\partial t} = -\nabla_3 \cdot (\bar{V}_M K_H + \Phi_H \bar{V}_{3H}) - \bar{V}_H \cdot (\bar{V}_{3H} \cdot \nabla_3 \bar{V}_M) - \omega_H \alpha_H - \bar{V}_H \cdot \overline{(\bar{V}_{3T} \cdot \nabla_3 \bar{V}_T)}^H + \bar{F}_{rH} \cdot \bar{V}_H \tag{3}$$

In (3),  $K_H = \frac{1}{2} |\bar{V}_H|^2$  represents the HF EKE;  $\omega$  and  $\alpha$  stand for vertical velocity in pressure coordinates and specific volume, respectively. The first term on the right hand side (RHS) of (3) is the convergence of the 3D energy flux (EFC), which includes the advection of HF EKE by the time-mean flow and the energy dispersion associated with ageostrophic geopotential flux. Note that the EFC term reduces to the net flux at the upper and lower boundaries when integrated over the entire atmosphere, and it mainly acts to redistribute EKE in the space. The second term on the RHS of (3) represents the conversion of kinetic energy from the time-mean flow to the HF eddies and is often referred to as barotropic conversion (BT). The third term on the RHS measures the rate of conversion from eddy potential energy (EPE) to EKE, also known as baroclinic conversion (BC). The fourth term is the production of HF EKE via cross-frequency eddy–eddy interaction (CFEI). The last term on the RHS of (3) is the mechanical dissipation of HF EKE. The CFEI term can be further divided by separating the total flow of transient eddies into the HF, IF and LF component, i.e.,

$$\begin{aligned} -\bar{V}_H \cdot \overline{(\bar{V}_{3T} \cdot \nabla_3 \bar{V}_T)}^H &= -\bar{V}_H \cdot \overline{(\bar{V}_{3H} \cdot \nabla_3 \bar{V}_H)}^H \\ &- \bar{V}_H \cdot \overline{(\bar{V}_{3H} \cdot \nabla_3 \bar{V}_I + \bar{V}_{3I} \cdot \nabla_3 \bar{V}_H + \bar{V}_{3I} \cdot \nabla_3 \bar{V}_I)}^H \\ &- \bar{V}_H \cdot \overline{(\bar{V}_{3H} \cdot \nabla_3 \bar{V}_L + \bar{V}_{3L} \cdot \nabla_3 \bar{V}_H + \bar{V}_{3L} \cdot \nabla_3 \bar{V}_L)}^H \\ &- \bar{V}_H \cdot \overline{(\bar{V}_{3I} \cdot \nabla_3 \bar{V}_L + \bar{V}_{3L} \cdot \nabla_3 \bar{V}_I)}^H \end{aligned} \tag{4}$$

In (4), the CFEI term now consists of 4 parts: kinetic energy generation due to interaction among HF eddies (HH, first term on the RHS of (4)), interaction between HF and IF eddies (HI, second term on the RHS of (4)), interaction between HF and LF eddies (HL, third term on the RHS of (4)), and interactions among HF, IF and LF eddies (HIL, last term on the RHS of (4)). A full list of the abbreviations and definitions is shown in table 1.

In a similar way, the IF EKE equation can be obtained, i.e.,

$$\frac{\partial K_I}{\partial t} = -\nabla_3 \cdot (\bar{V}_M K_I + \Phi_I \bar{V}_{3I}) - \bar{V}_I \cdot (\bar{V}_{3I} \cdot \nabla_3 \bar{V}_M) - \omega_I \alpha_I - \bar{V}_I \cdot \overline{(\bar{V}_{3T} \cdot \nabla_3 \bar{V}_T)}^I + \bar{F}_{rI} \cdot \bar{V}_I \tag{5}$$

where

$$\begin{aligned} -\bar{V}_I \cdot \overline{(\bar{V}_{3T} \cdot \nabla_3 \bar{V}_T)}^I &= -\bar{V}_I \cdot \overline{(\bar{V}_{3I} \cdot \nabla_3 \bar{V}_I)}^I \\ &- \bar{V}_I \cdot \overline{(\bar{V}_{3H} \cdot \nabla_3 \bar{V}_I + \bar{V}_{3I} \cdot \nabla_3 \bar{V}_H + \bar{V}_{3H} \cdot \nabla_3 \bar{V}_H)}^I \\ &- \bar{V}_I \cdot \overline{(\bar{V}_{3I} \cdot \nabla_3 \bar{V}_L + \bar{V}_{3L} \cdot \nabla_3 \bar{V}_I + \bar{V}_{3L} \cdot \nabla_3 \bar{V}_L)}^I \\ &- \bar{V}_I \cdot \overline{(\bar{V}_{3H} \cdot \nabla_3 \bar{V}_L + \bar{V}_{3L} \cdot \nabla_3 \bar{V}_H)}^I \end{aligned} \tag{6}$$

Table 2 presents a full list of the abbreviations and definitions used in discussing the IF EKE budget. Note that the CFEI terms presented here do not represent direct transfers of EKE among eddies residing in different frequency bands. For example, HI in the HF EKE equation quantifies the production of HF EKE due to the interaction between HF and IF eddies and it is not the direct opposite to the HI in the IF EKE equation which represents the generation of IF EKE due to the interaction between HF and IF eddies. The complete set of EKE equations including the so-called “cross-terms” are provided in the appendix of this paper for the reader’s reference.

The budget analysis for HF and IF EKE is based upon Eqs. (3–6) and uses the NCEP-DOE Reanalysis for the period 1979 to 2011. This dataset consists of standard daily atmospheric fields such as horizontal and vertical wind, geopotential height and temperature on 17 pressure levels and a 2.5° latitude × 2.5° longitude grid (Kanamitsu et al. 2002). Monthly sea surface temperature (SST) in the Nino 3.4 region is obtained from the NOAA Climate Prediction

**Table 1** Abbreviations and definitions of the HF EKE budget

Abbreviations	HF EKE	EFC	BT	BC	CFEI
Formula	$\frac{1}{2}  \bar{V}_H ^2$	$-\nabla_3 \cdot (\bar{V}_M K_H + \Phi_H \bar{V}_{3H})$	$-\bar{V}_H \cdot (\bar{V}_{3H} \cdot \nabla_3 \bar{V}_M)$	$-\omega_H \alpha_H$	$-\bar{V}_H \cdot \overline{(\bar{V}_{3T} \cdot \nabla_3 \bar{V}_T)^H}$
Definition	HF eddy kinetic energy	Energy flux convergence	Barotropic conversion	Baroclinic conversion	Cross-frequency eddy–eddy interaction

**Table 2** Abbreviations and definitions of the IF EKE budget

Abbreviations	IF EKE	EFC	BT	BC	CFEI
Formula	$\frac{1}{2}  \bar{V}_I ^2$	$-\nabla_3 \cdot (\bar{V}_M K_I + \Phi_I \bar{V}_{3I})$	$-\bar{V}_I \cdot (\bar{V}_{3I} \cdot \nabla_3 \bar{V}_M)$	$-\omega_I \alpha_I$	$-\bar{V}_I \cdot \overline{(\bar{V}_{3T} \cdot \nabla_3 \bar{V}_T)^I}$
Definition	IF eddy kinetic energy	Energy flux convergence	Barotropic conversion	Baroclinic conversion	Cross-frequency eddy–eddy interaction

Center (CPC, <http://www.cpc.ncep.noaa.gov/data/indices/>) to identify El Niño and La Niña events in the composite analysis. A Lanczos filter (Duchon 1979) with 203 weights is used throughout the analysis to separate transient eddies into different frequency bands and to conduct corresponding bandpass filtering for the CFEI term. The choice of 203 weights guarantees the tradeoff between Gibbs effect and the sharpness of stop-band. Mass-weighted vertical averaging between 1,000 and 200 mb is done for part of the results to highlight the horizontal distribution of EKE budget terms in the troposphere. Standard regression analysis and Student's *t* test are used to identify significant ENSO-induced anomalies in the EKE budget.

### 3 Results

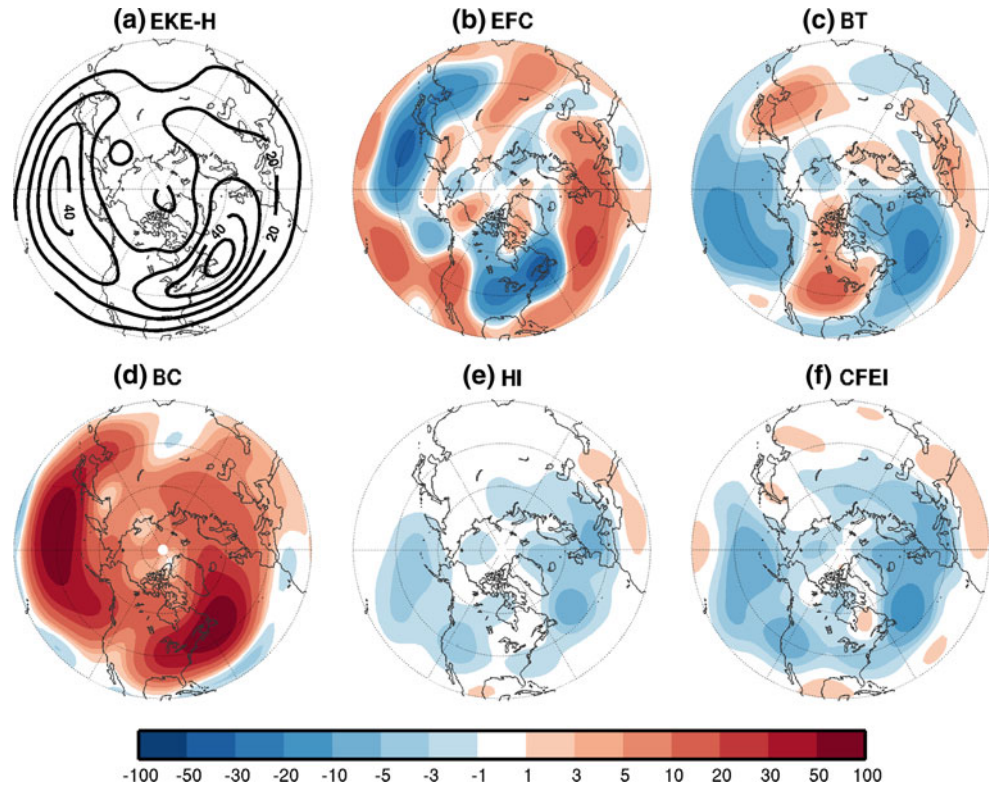
#### 3.1 Climatology

The winter (December–January–February, DJF) climatology of the HF EKE and the related energy conversion terms are shown in Fig. 1. All quantities displayed are mass-weighted tropospheric averages. The two localized maxima in the HF EKE field (Fig. 1a) correspond to the two distinct storm tracks over the North Pacific and North Atlantic in boreal winter with the Atlantic storm track being more intense compared to the Pacific one (e.g., Chang et al. 2002). The EFC term in the HF EKE budget (Fig. 1b) is characterized by a west–east dipole over both basins. This spatial structure indicates that mean-flow advection and energy dispersion via ageostrophic geopotential flux effectively redistribute EKE eastward and extend the storm tracks to the east ocean basins where local baroclinicity is relatively weak compared to the west ocean basins, a process known as “downstream development”

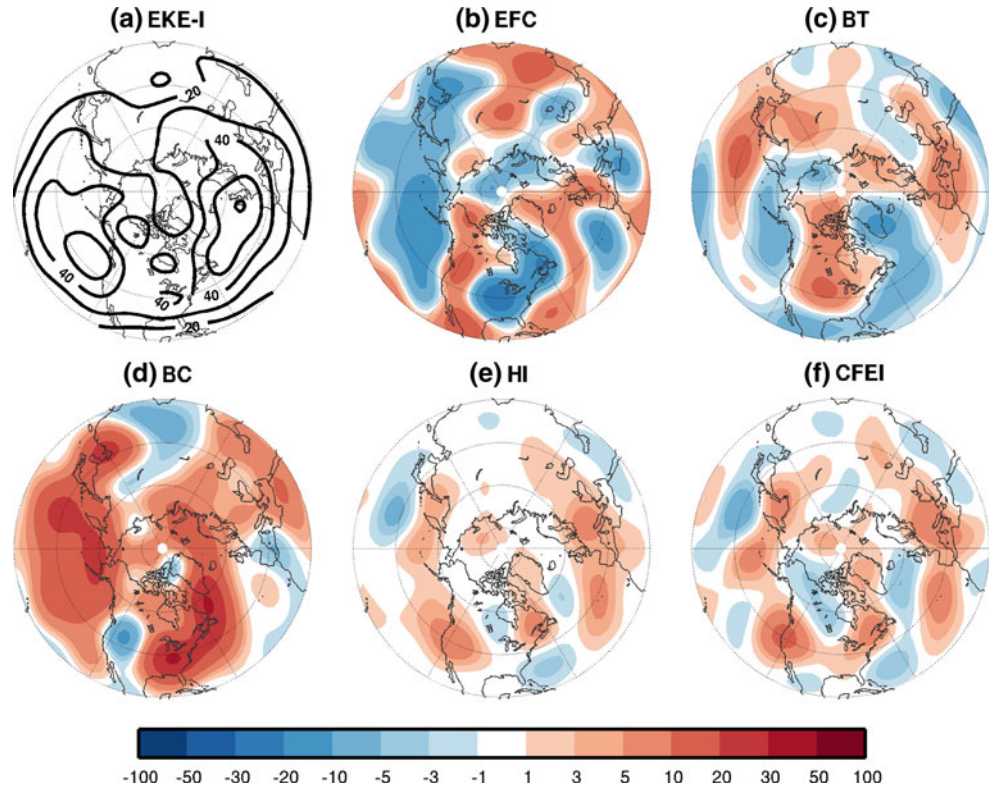
(Mak and Cai 1989; Chang 1993). The values of barotropic conversion (BT, Fig. 1c) are generally negative over the North Pacific and North Atlantic, and are positive over East Asia, North America and North Africa, consistent with previous findings that HF eddies gain (lose) kinetic energy from (to) the background flow as they propagate toward (away from) a localized jet and become more isotropic (anisotropic) in the confluent (diffluent) region of the jet entrance (exit) (e.g., Wallace and Lau 1985; Cai et al. 2007; Deng and Mak 2006). The close match between local maxima in baroclinic conversion (BC, Fig. 1d) and those in HF EKE field (Fig. 1a) clearly demonstrates that BC is the primary process generating HF EKE. Figure 1f show the distribution of EKE production due to nonlinear interaction among eddies of different timescales, i.e., the CFEI term. The net effect of CFEI is to decrease HF EKE over the eastern North Pacific and the entire North Atlantic. This is a clear demonstration that nonlinear, scale–interaction processes are more important over regions where synoptic waves attain large amplitudes. The main contributor to the CFEI term is the interaction between HF and IF eddies, i.e., HI, shown in Fig. 1e.

Figure 2 shows the climatological budget terms for IF EKE. The maxima in IF EKE (Fig. 2a) are located downstream of the respective storm tracks as indicated by the maxima in HF EKE (Fig. 1a). The larger magnitude of IF EKE compared to HF EKE is consistent with the result of Sheng and Hayashi (1990a) that the peak transient eddy kinetic energy is found in the period ranging from 6.8 to 34 days, roughly corresponding to our definition of the IF band. The horizontal distribution of EFC (Fig. 2b) is characterized by two dipoles. Over the North Pacific, EFC reduces IF EKE over the entire basin and increases EKE over western North America. Negative (positive) EFC values are also found over eastern North America (North

**Fig. 1** Winter climatology of the tropospheric-averaged EKE budget for HF eddies. **a** HF EKE (contour interval:  $10 \text{ m}^2/\text{s}^2$ ); **b** EFC; **c** BT; **d** BC; **e** HI; **f** CFEI. Units in **b–f** are  $\text{m}^2\text{s}^{-2}/\text{day}$ . All data have been spectrally truncated to T15 before plotting. For detailed definitions of various budget terms, please refer to Table 1



**Fig. 2** Same as Fig. 1, except for IF eddies; for detailed definitions, please refer to Table 2



Atlantic). Similar to that in the HF EKE budget, BT (Fig. 2c) shows three centers of positive conversion upstream of the winter time-mean jets (East Asia-Western Pacific, North America and North Africa) and three centers

of negative conversion downstream of the jets (eastern North Pacific, North Atlantic and East Europe). BC (Fig. 2d) still contributes substantially to the production of IF EKE in the northern midlatitudes.

Over a large portion of the North Pacific, the effects of BC, EFC and BT cancel out. This leaves CFEI (Fig. 2f) to stand out, especially over the eastern North Pacific and western North America, where HI (Fig. 2e) dominates the CFEI term and overlaps with the maximum of IF EKE. The significant contribution to IF EKE from the interaction between HF and IF eddies (i.e., the HI term) confirms the critical role of synoptic eddies in the development and maintenance of IF disturbances such as a blocking high or a cutoff low (e.g., Cai and Van Den Dool 1994). Note that the HI term does not quantify the direct kinetic energy transfer between HF and IF eddies. Over the eastern North Atlantic and West Europe, the northern portion of the IF EKE maximum is largely determined by the effect of EFC while the southern portion is collectively contributed by BT and CFEI (primarily HI). The positive BT contribution here supports the idea that some IF eddies might originate from barotropic instability of a zonally-varying background flow (for a review, please see Dole 2008). These results suggest that the characteristics of IF EKE budget are fundamentally different between the two ocean basins. Additionally, our analysis also suggests that the interaction among IF eddies themselves, i.e., the II term (not shown due to small values), has little contribution to the lifecycle of IF disturbance as discussed earlier by Cash and Lee (2000).

To delineate the vertical structure of the EKE budget, we present here also the zonal mean of the various

conversion terms. Figure 3 shows the corresponding latitude-pressure cross-sections for the zonal mean quantities in the HF EKE budget. The maximum HF EKE (Fig. 3a, contours) is found in the upper troposphere around 300 mb with peak amplitude exceeding  $30 \text{ J m}^{-3}$ . It is located on the northern flank of the tropospheric zonal-mean zonal jet (Fig. 3a, shading). In the sense of zonal mean, the primary role of EFC process (Fig. 3b) is to vertically redistribute HF EKE, which is mainly produced by BC (Fig. 3d) in the mid-lower troposphere (below 500 mb). This redistribution process leads to the HF EKE maximum in the upper troposphere; meanwhile, part of the EKE is dispersed to lower levels where mechanical dissipation in the boundary layer removes EKE. The damping of HF EKE by barotropic processes (BT) is strongest around 500 mb and located primarily on the northern flank of the zonal jet (Fig. 3c). CFEI (Fig. 3f) is another major sink of HF EKE in the midlatitudes, and the largest negative conversion, due to interaction between HF and IF eddies, is found in the middle troposphere ( $\sim 500 \text{ mb}$ ) directly beneath the center of maximum EKE. The vertical structure of HI is similar to that of BT indicating the same physical nature of the two conversion processes, i.e., both related to Reynolds stresses.

For the IF EKE, the maximum in its zonal mean is located to the north of and slightly above the jet core with peak amplitude exceeding  $40 \text{ J m}^{-3}$  (Fig. 4a, contours). Similar to that in the HF EKE budget, the effect of BC is

**Fig. 3** Latitude-pressure cross-sections of the climatological zonal-mean EKE budget terms for HF eddies. All terms have been mass-weighted by multiplying the air density. Contours are HF EKE (contour interval:  $5 \text{ J m}^{-3}$ ). Color shading in a–i correspond to a zonal wind; b EFC; c BT; d BC; e HI; f CFEI. Unit is  $\text{ms}^{-1}$  in (a) and  $\text{J m}^{-3}/\text{day}$  in (b–f)

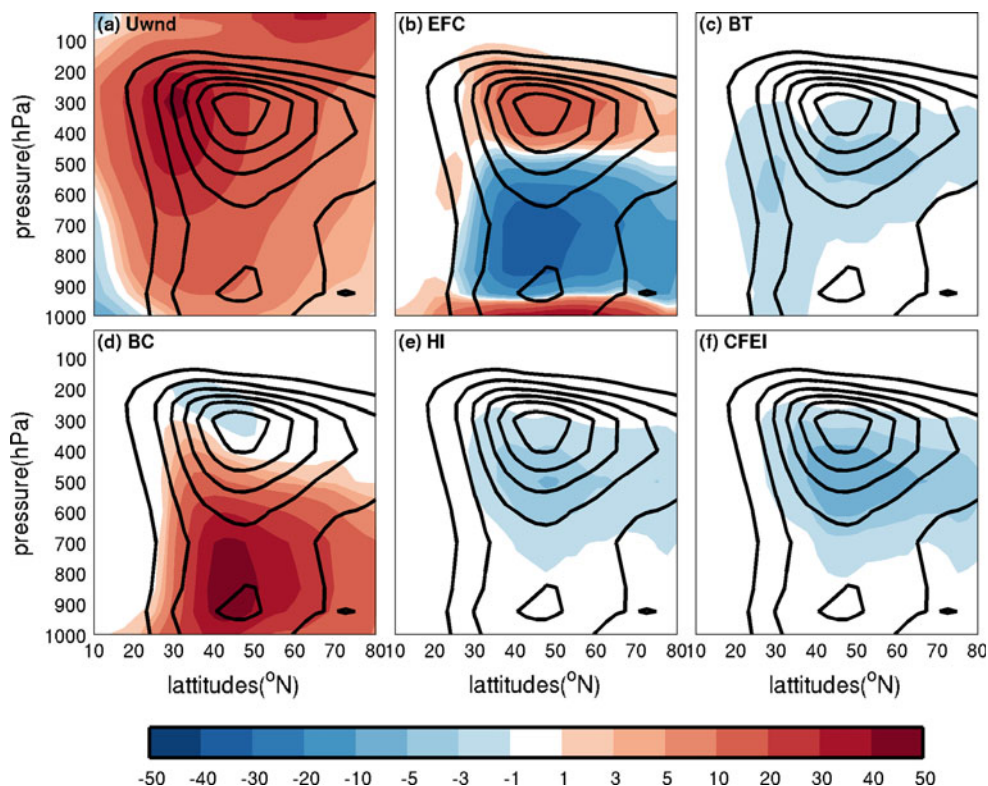
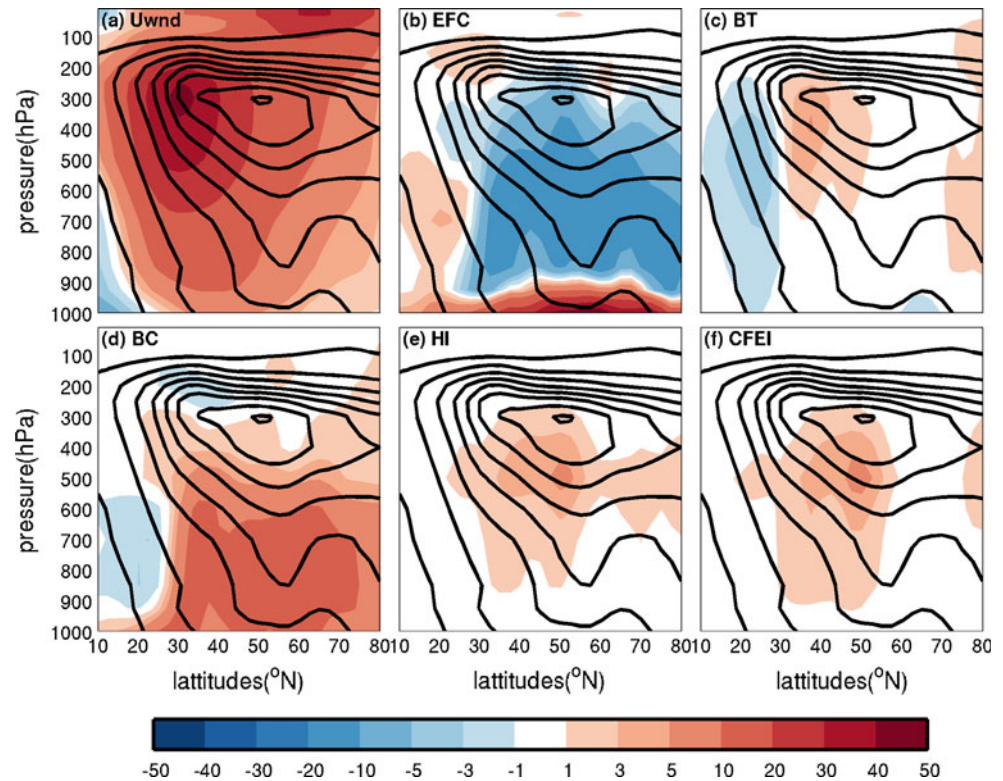


**Fig. 4** Same as Fig. 3 except for IF eddies



still concentrated below 500 mb (Fig. 4d). The effect of BC is largely balanced by the effect of EFC (Fig. 4b). In the zonal-mean sense, the role of BT in the IF and HF EKE budget is distinctly different. BT represents an important sink of HF EKE (Fig. 3c), but only does so for IF EKE on the southern flank (equatorward side) of the zonal-mean jet. On the northern flank and near the level of maximum IF EKE, BT acts as a primary source of IF EKE. Given the strong cancellation between BC and EFC, the positive EKE productions due to BT and CFEI (dominated by HI, Fig. 4f, e) turn BT and HI into the two most important contributors to IF EKE when the zonal-mean budget is considered.

In addition to the zonal mean, we also examine longitude-pressure cross-sections of meridionally-averaged (over  $30^{\circ}\text{N}$ – $60^{\circ}\text{N}$ ) quantities. Fig. 5 shows the corresponding budget terms for HF eddies. The zonal distribution of HF EKE clearly reveals two distinct storm tracks over the North Pacific and North Atlantic (Fig. 5a, contour). EFC (Fig. 5b) redistributes part of the HF EKE generated by BC (Fig. 5d) in the lower-mid troposphere to upper levels and is responsible for the formation of the upper tropospheric maximum in EKE. The two lower-tropospheric maxima in HF EKE are located over the west ocean basins adjacent to the east coasts of the Asian and North American continent, where near surface baroclinicity and BC tend to peak (Fig. 5d). In Fig. 6, EFC is further separated into energy convergence due to (horizontal and vertical) mean-flow advection and due to (horizontal and vertical) ageostrophic

geopotential flux. It is clear that the convergence due to ageostrophic geopotential flux, particularly its vertical component (Fig. 6d), is the dominant process of EFC in the HF EKE budget. The horizontal components of the mean-flow advection (Fig. 6a) and EKE dispersion (Fig. 6b) reach their respective maximum values in the upper troposphere. As in the zonal mean case, BT (Fig. 5c) and CFEI (mainly HI, Fig. 5f, e) serve as two major sinks of HF EKE.

The counterpart longitude-pressure cross-sections for IF EKE budget terms are shown in Fig. 7. Consistent with the zonal mean quantities, BT (Fig. 7c) acts as an important source of IF EKE directly contributing to the formation of the two upper-tropospheric maxima over the east ocean basins. BC has non-negligible contributions to the upper-tropospheric EKE maxima, although the main positive conversions associated with BC are still found in the lower troposphere over the west ocean basins (Fig. 7d). The overall impact of EFC in determining the upper-tropospheric maxima of IF EKE is relatively small compared to that in the HF EKE budget. Further breakdown of the EFC term indicates that it is also dominated by the energy convergence due to the vertical component of the geopotential flux (figure not shown). CFEI (Fig. 7f), another critical source of IF EKE, is mainly contributed by the EKE generation due to interaction between HF and IF eddies (HI, Fig. 7e). The zonal and vertical distribution of HI indicates that such nonlinear interactions preferentially occur in the mid-upper troposphere over Eastern Pacific-

**Fig. 5** Longitude-pressure cross-sections of the climatological HF EKE budget terms meridionally averaged between 30°N and 60°N. All terms have been mass-weighted by multiplying the air density. Contours are HF EKE (contour interval:  $5 \text{ J m}^{-3}$ ). Color shading in (a–i) correspond to **a** zonal wind; **b** EFC; **c** BT; **d** BC; **e** HI; **f** CFEI. Unit is  $\text{ms}^{-1}$  in (a) and  $\text{J m}^{-3}/\text{day}$  in (b–i)

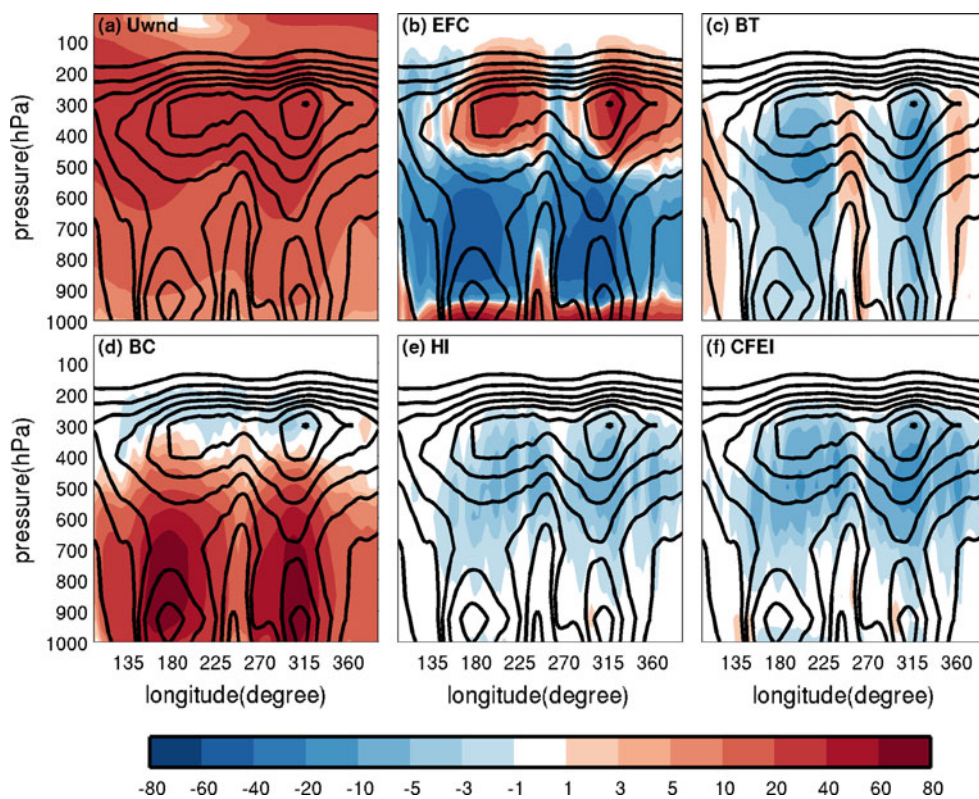
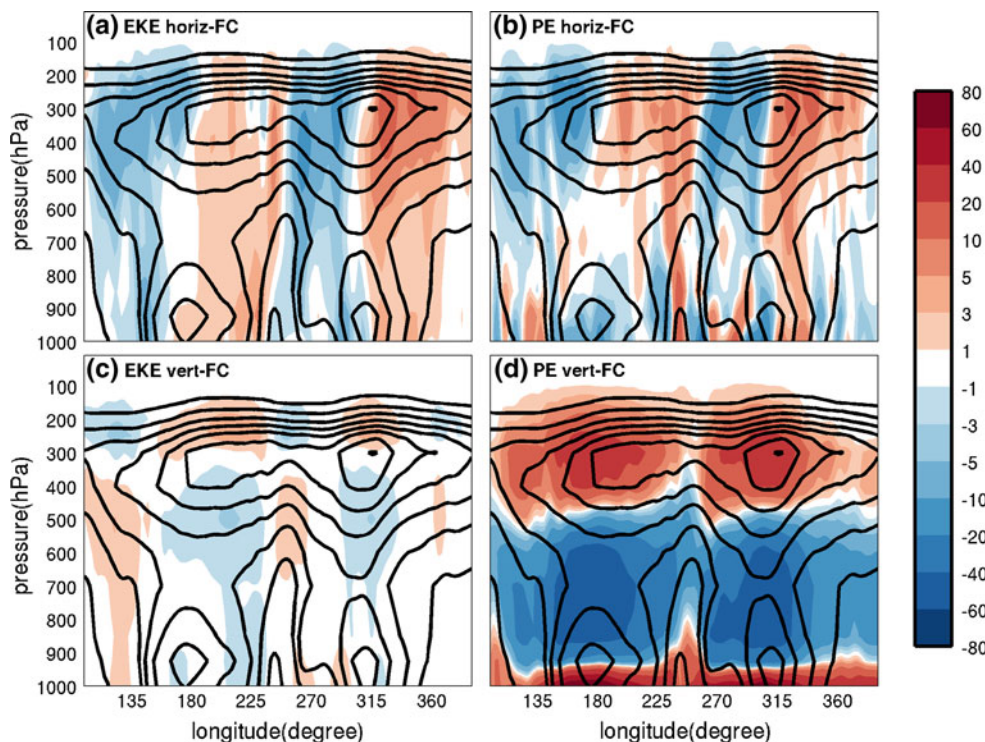


**Fig. 6** Longitude-pressure cross-sections of the HF EKE convergence due to horizontal advection of EKE by the winter-mean flow (a), horizontal ageostrophic geopotential flux (b), vertical advection of EKE by the winter-mean flow (c), and vertical ageostrophic geopotential flux (d). All terms have been mass-weighted by multiplying the air density. Contours are HF EKE (contour interval:  $5 \text{ J m}^{-3}$ ). All quantities shown are meridional-averages between 30°N and 60°N. Unit is  $\text{J m}^{-3}/\text{day}$

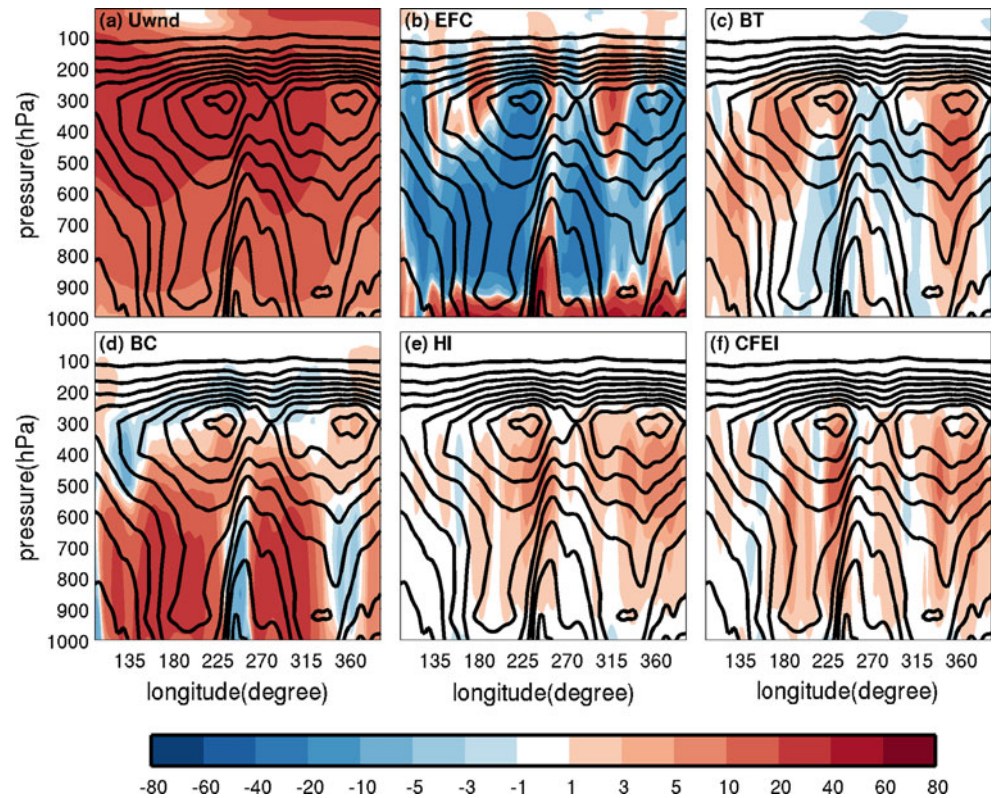


Western North America and over Eastern Atlantic-Western Europe. Both regions are characterized by an elevated activity of atmospheric blocking. The positive role played by HI in the IF EKE budget therefore provides additional

evidence that synoptic-scale transients and eddy–eddy interactions are an integral part of the dynamics of atmospheric blocking (e.g. Egger 1978; Shutts 1983, 1986; Nakamura and Wallace 1990, 1993; Nakamura et al. 1997).



**Fig. 7** Same as Fig. 5 except for IF eddies



Consequently, one of the potential applications of the local energetics diagnosis presented here is model evaluations that seek to identify sources of biases and improve the representation of blocking events in a global model.

### 3.2 Interannual variability

The interannual variability of the various energy conversion terms constitutes an important aspect of the EKE budget. We first quantify the overall amplitude of the interannual variation in various budget terms in terms of the standard deviation of their respective DJF-mean values. Figure 8 presents the results for HF eddies. The maximum standard deviations of EFC, BC and BT, shown in Fig. 8b, c, d, respectively, are located downstream of the corresponding time-mean jets over the western North Pacific and western North Atlantic. The maximum interannual variability of CFEI (Fig. 8f) is found over the eastern North Pacific and over the western North Atlantic. Over both basins, EFC exhibits the largest interannual variability among all the budget terms. The magnitudes of interannual variations in terms of standard deviations are generally larger over the North Atlantic than those over the North Pacific, likely a result of larger eddy amplitudes in the former region. On average, interannual variability represents approximately 20–70 % changes with respect to the local climatological values.

The overall spatial structure of the interannual variability in the IF EKE budget terms (Fig. 9) is similar to that

of the HF EKE budget terms in the sense that the maximum variability tends to overlap with the maximum climatological values of the respective terms. For IF eddies, EFC shows the largest amplitude of interannual variation among all the budget terms, and it is equivalent to more than 100 % changes with respect to the climatological values over Gulf of Alaska and the North Atlantic (Fig. 9b). The interannual variability of BT (Fig. 9c) in the IF EKE budget shares similar spatial patterns with that in the HF EKE budget (Fig. 8c) but with a larger amplitude. The amplitude of the interannual variability of BC, on the other hand, is weaker for IF eddies (Fig. 9d) compared to that for HF eddies (Fig. 8d). The standard deviations of the CFEI term turn out to be large for both HF and IF eddies (Figs. 8i, 9i). A distinction between the HF and IF eddies is that the magnitude of the interannual variability of the interaction among eddies of similar scales, i.e., HH (Fig. 8e) and II (Fig. 9e), is quite different. II clearly varies more substantially on a year-to-year basis compared to HH.

ENSO represents the most prominent signal of interannual variability in the Earth's climate system and has profound impacts on global atmospheric circulation (e.g., Bjerknes 1969; Trenberth et al. 1998). To investigate the influence of ENSO on local EKE budgets, we regress DJF-mean values of the zonally- and vertically-averaged energy conversion terms onto the Nino3.4 index. The longitudinal sectors for zonal averaging is chosen based on regions exhibiting maximum interannual variability as shown in

**Fig. 8** Interannual standard deviations of the HF EKE budget terms in winter season. **a** HF EKE (contour interval:  $10 \text{ m}^2/\text{s}^2$ ); **b** EFC; **c** BT; **d** BC; **e** HH; **f** HI; **g** HL; **h** HIL; **i** CFEI. Units in (b–i) are  $\text{m}^2 \text{ s}^{-2}/\text{day}$ . All data have been spectrally truncated to T15 before plotting. For detailed definitions of various budget terms, please refer to Table 1

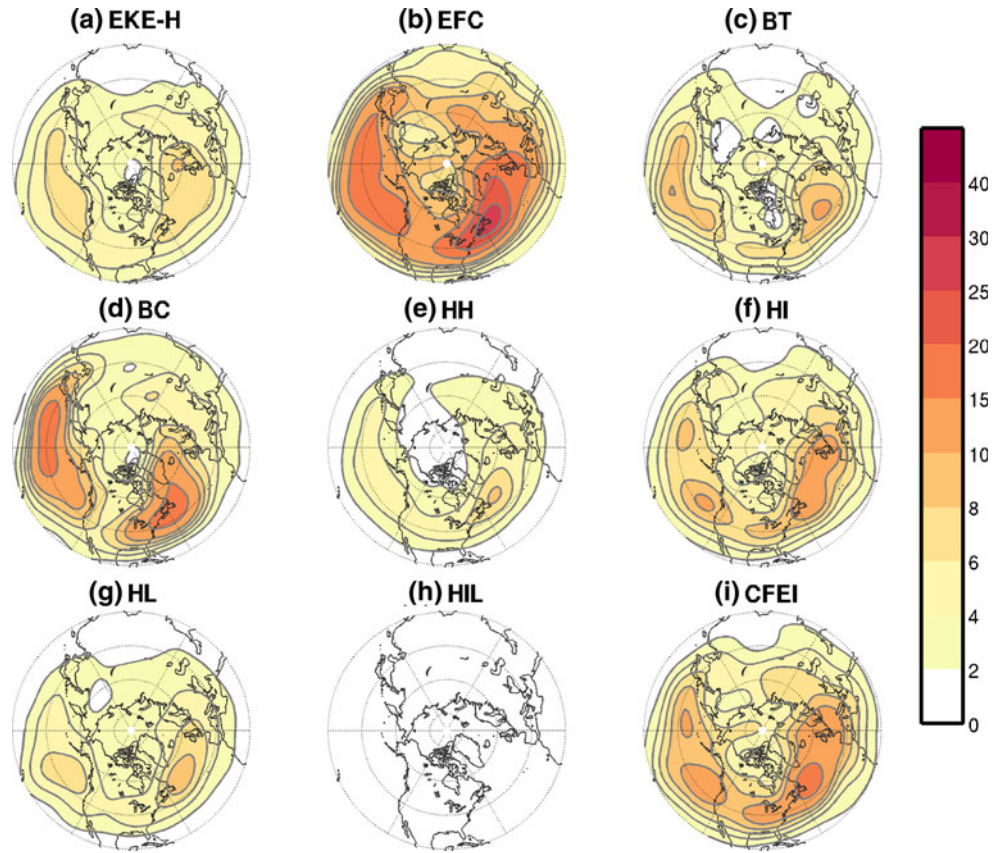
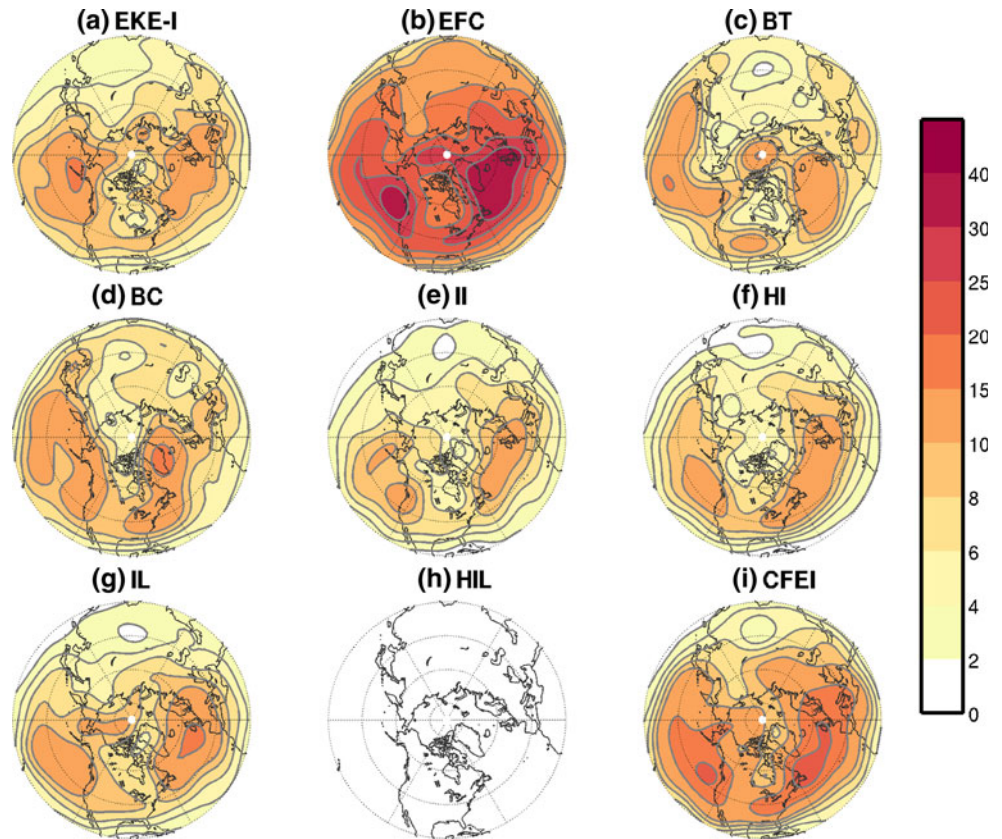


**Fig. 9** Interannual standard deviations of the IF EKE budget terms in winter season. **a** IF EKE (contour interval:  $10 \text{ m}^2/\text{s}^2$ ); **b** EFC; **c** BT; **d** BC; **e** II; **f** HI; **g** IL; **h** HIL; **i** CFEI. Units in (b–i) are  $\text{m}^2 \text{ s}^{-2}/\text{day}$ . All data have been spectrally truncated to T15 before plotting. For detailed definitions of various budget terms, please refer to Table 2



Figs. 8 and 9. The meridional distribution of the regression coefficients for the HF EKE budget terms are plotted in Fig. 10. A meridional dipole in the regression coefficients for HF EKE over the North Pacific (thick black line in Fig. 10a) indicates an equatorward shift of the Pacific storm track during El Niño winters as discussed in previous studies (e.g., Trenberth and Hurrell 1994). The elevated level of EKE on the equatorward side of the climatological storm track is accompanied by a southward shift of the maximum BC (red line in Fig. 10a) and positive anomalies of BT around 35°N (cyan line in Fig. 10a). The decrease of HF EKE to the north is a result of negative conversion anomalies in BC. In contrast, both EFC (thin black line in Fig. 10a) and CFEI (magenta line in Fig. 10a) work against the observed pattern of EKE anomalies meaning positive (negative) EFC and EFC anomalies are found where EKE anomalies are negative (positive).

Over the North Atlantic, the ENSO response in the HF EKE field is characterized by a tri-pole anomaly with decreased EKE in midlatitudes (around 50°N) and increased EKE in subtropics and high latitude regions

(thick black line in Fig. 10b). Note that due to the southwest-northeast tilt of the North Atlantic storm track, zonal averaging tends to smooth out the signal. The results presented in Fig. 10b are thus a slight underestimate of the actual response. The tri-pole anomaly in HF EKE over the North Atlantic is largely induced by anomalies in BC (red line in Fig. 10b) and CFEI (magenta line in Fig. 10b). Similar to that over the North Pacific, EFC tends to work against this tri-pole anomaly (thin black line in Fig. 10b). BT (cyan line in Fig. 10b) also works against the decrease of HF EKE around 50°N. Comparing the response of the eddy–eddy interaction term over the two oceanic basins, we find that HI (green line in Fig. 10a) dominates the response of CFEI over the North Pacific while both HI (green line in Fig. 10b) and HL (blue line in Fig. 10b) are relevant for the CFEI response over the North Atlantic.

The corresponding results for IF EKE are shown in Fig. 10c and d. In response to El Niño events, IF EKE generally decreases across the North Pacific between 30°N and 70°N with the maximum decrease found around 45°N (thick black line in Fig. 10c). Similar to the HF EKE over

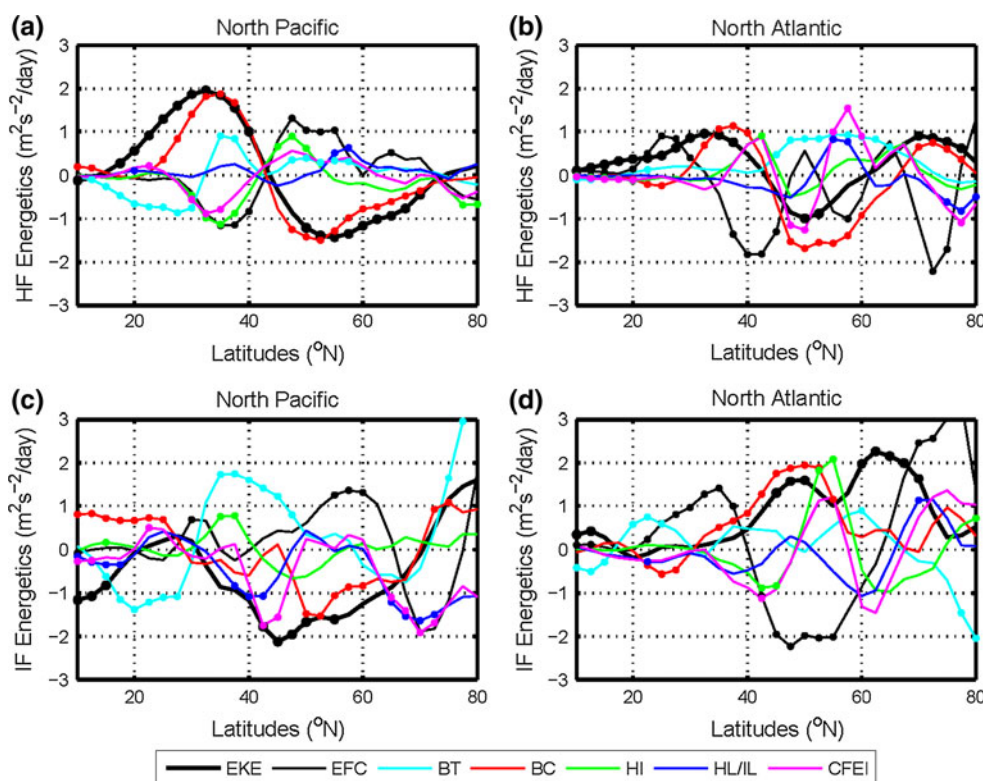


**Fig. 10** Response of the EKE budget terms to ENSO forcing in terms of coefficients obtained by regressing the corresponding budget terms onto the monthly Nino3.4 index. **a** HF EKE budget terms that are zonally-averaged over the North Pacific basin (140°E–120°W) and mass-weighted, vertically-averaged in the troposphere; **b** HF EKE budget terms that are zonally-averaged over the North Atlantic basin (90°W–0°E) and mass-weighted, vertically-averaged in the troposphere. **c** IF EKE budget terms that are zonally-averaged over the North Pacific basin (160°E–110°W) and mass-weighted, vertically-

averaged in the troposphere. **d** IF EKE budget terms that are zonally-averaged over the North Atlantic basin (60°W–30°E) and mass-weighted, vertically-averaged in the troposphere. The EFC term in IF EKE budget **c** and **d** is scaled by 0.5 to fit the panels. The blue solid lines in **(a)** and **(b)** represent HL in the HF EKE budget; while in **(c)** and **(d)** they represent IL in the IF EKE budget. The unit for EKE anomalies is  $m^2 s^{-2}/K$ , and  $m^2 s^{-2} day^{-1} K^{-1}$  for rest of the terms. Results passed the 80 % significance level are marked with filled circle

the North Pacific, the suppressed IF EKE is clearly associated with negative anomalies of BC (red line in Fig. 10c) north of 50°N and EFC (thin black line in Fig. 10b) works against the observed EKE anomalies in the midlatitudes. In contrast to the HF EKE, the suppression of IF EKE is also tied to negative anomalies of CFEI (magenta line in Fig. 10c), which is dictated by changes in IL (blue line in Fig. 10c) between 40°N and 50°N. Unlike that in the HF EKE budget, the effect of BT in the IF EKE budget (cyan line in Fig. 10c) tends to work against the IF EKE anomalies at low and mid-latitudes, while it is clearly contributing positively to the IF EKE anomalies north of 65°N.

In contrast to the North Pacific, IF EKE generally increases over the North Atlantic in El Niño winters and the maximum increase is located between 40°N and 70°N (thick black line in Fig. 10d). This increase is largely contributed by a positive BC anomaly (red solid line in Fig. 10d) between 40°N and 60°N while CFEI (magenta line in Fig. 10d) and BT (cyan line in Fig. 10d) also play some roles north of 50°N. The CFEI response receives similar contributions from HI (green line in Fig. 10d) and IL (blue line in Fig. 10d) north of 50°N. EFC term (thin black line in Fig. 10d), on the other hand, still works against the observed EKE anomalies, particularly between 40°N and 70°N.

#### 4 Concluding remarks

In this study, we quantify the winter climatology, interannual variability, and ENSO response of the local kinetic energy budget terms for both the HF and IF eddies. HF eddies depict extratropical storm tracks that are responsible for day-to-day weather variability in northern winter while IF eddies represent the class of relatively low-frequency disturbances giving rise to phenomena such as atmospheric blocking and teleconnections. By adopting a new form of the EKE equation, we are able to isolate the effect of EKE generation/destruction due to interactions among eddies of different timescales. The so-called CFEI term is a significant sink of HF EKE and a major source of IF EKE over both the North Pacific and North Atlantic basins. The results of local energetics, presented in the forms of both tropospheric-average and latitude/longitude-pressure cross-sections, confirm findings in earlier studies that synoptic-scale disturbances contribute positively to the onset and maintenance of extratropical atmospheric low-frequency variability, particularly over the eastern ocean basins. In the winter climatology, BT is most active in the mid and upper troposphere while BC is concentrated below 500 mb. BC contributes positively to both HF and IF EKE while BT often damps HF EKE and enhances IF EKE. The mean-flow advection of EKE and kinetic energy dispersion,

captured in the EFC term, are always important in determining the final 3D distribution of EKE in the troposphere.

Substantial interannual variations are found in the HF and IF EKE budget terms. The HF EKE response to warm events of ENSO is characterized by a dipole anomaly over the North Pacific and a tri-pole anomaly over the North Atlantic. BC is the main driver of the observed changes in HF EKE while BT, CFEI and EFC all play non-negligible roles in determining the final meridional structure of the HF EKE anomalies. The impact of ENSO on IF EKE is different between the two ocean basins: IF EKE generally decreases over the North Pacific and increases over the North Atlantic. For HF EKE, among all the eddy–eddy interaction terms, HI dictates the CFEI response to ENSO over the North Pacific while both HI and HL are important over the North Atlantic. For IF EKE, IL dominates the CFEI response over the North Pacific, and HI and IL are both relevant over the North Atlantic.

The results presented here demonstrate that in terms of local energetics, IF eddies are more complicated compared to HF eddies. Proper representations of IF eddies in a model is critical for medium-range forecasts (e.g., Reinhold 1987), even in the simulation of regional hydrological extremes like atmospheric rivers (ARs) (e.g., Jiang and Deng 2011). The contrasts between the North Pacific and North Atlantic basin are particularly pronounced in terms of the ENSO response of the HF and IF EKE budget terms. Diagnosing local energetics of transient eddies of various timescales thus can serve as an efficient tool for identifying sources of differences in general circulation features among various reanalysis datasets and model simulations. Finally, it is important to recognize here that kinetic energy budget represents only one part of the total eddy energy budget. Future work will include a counterpart analysis on the potential energy of eddies of different timescales and also evaluations of eddy energy budget in the next generation climate models.

**Acknowledgments** We thank two anonymous reviewers for their thoughtful comments and suggestions that led to major improvements of the manuscript. The NCEP-DOE Reanalysis used in this study were provided through <http://www.esrl.noaa.gov/psd/data/gridded/data.ncep.reanalysis2.html>. This research was supported by the NASA Energy and Water Cycle Study (NEWS) under Grant NNX09AJ36G and by DOE Office of Science Regional and Global Climate Modeling (RGCM) program under Grant DE-SC0005596.

#### Appendix

Listed below is the complete set of equations, including kinetic energy equations for HF, IF, LF eddies and the winter-mean flow, and equations for the cross-terms.

$$\frac{\partial K_H}{\partial t} = -\nabla_3(\bar{V}_{3M}K_H + \bar{V}_{3H}\Phi_H) - \bar{V}_H \cdot (\bar{V}_{3H} \cdot \nabla_3 \bar{V}_M) - \bar{V}_H \cdot (\bar{V}_{3T} \cdot \nabla_3 \bar{V}_T) + \omega_H \alpha_H + \bar{V}_H \cdot \bar{F}_{rH}$$

$$\frac{\partial \bar{K}_I}{\partial t} = -\nabla_3(\bar{V}_{3M}K_I + \bar{V}_{3I}\Phi_I) - \bar{V}_I \cdot (\bar{V}_{3I} \cdot \nabla_3 \bar{V}_M) - \bar{V}_I \cdot (\bar{V}_{3T} \cdot \nabla_3 \bar{V}_T) + \omega_I \alpha_I + \bar{V}_I \cdot \bar{F}_{rI}$$

$$\frac{\partial \bar{K}_L}{\partial t} = -\nabla_3(\bar{V}_{3M}K_L + \bar{V}_{3L}\Phi_L) - \bar{V}_L \cdot (\bar{V}_{3L} \cdot \nabla_3 \bar{V}_M) - \bar{V}_L \cdot (\bar{V}_{3T} \cdot \nabla_3 \bar{V}_T) + \omega_L \alpha_L + \bar{V}_L \cdot \bar{F}_{rL}$$

$$\frac{\partial \bar{K}_M}{\partial t} = -\nabla_3(\bar{V}_{3M}K_M + \bar{V}_{3M}\Phi_M) - \bar{V}_M \cdot (\bar{V}_{3T} \cdot \nabla_3 \bar{V}_T) + \omega_M \alpha_M + \bar{V}_M \cdot \bar{F}_{rM}$$

$$\frac{\partial \bar{V}_H \cdot \bar{V}_I}{\partial t} = -\nabla_3 \cdot [(\bar{V}_H \cdot \bar{V}_I)\bar{V}_{3M} + \bar{V}_{3I}\Phi_H + \bar{V}_{3H}\Phi_I] - \bar{V}_I \cdot (\bar{V}_{3H} \cdot \nabla_3 \bar{V}_M) - \bar{V}_H \cdot (\bar{V}_{3I} \cdot \nabla_3 \bar{V}_M) - \bar{V}_I \cdot (\bar{V}_{3T} \cdot \nabla_3 \bar{V}_T) - \bar{V}_H \cdot (\bar{V}_{3T} \cdot \nabla_3 \bar{V}_T) + \omega_I \alpha_H + \omega_H \alpha_I + \bar{V}_I \cdot \bar{F}_{rH} + \bar{V}_H \cdot \bar{F}_{rI}$$

$$\frac{\partial \bar{V}_H \cdot \bar{V}_L}{\partial t} = -\nabla_3 \cdot [(\bar{V}_H \cdot \bar{V}_L)\bar{V}_{3M} + \bar{V}_{3L}\Phi_H + \bar{V}_{3H}\Phi_L] - \bar{V}_L \cdot (\bar{V}_{3H} \cdot \nabla_3 \bar{V}_M) - \bar{V}_H \cdot (\bar{V}_{3L} \cdot \nabla_3 \bar{V}_M) - \bar{V}_L \cdot (\bar{V}_{3T} \cdot \nabla_3 \bar{V}_T) - \bar{V}_H \cdot (\bar{V}_{3T} \cdot \nabla_3 \bar{V}_T) + \omega_L \alpha_H + \omega_H \alpha_L + \bar{V}_L \cdot \bar{F}_{rH} + \bar{V}_H \cdot \bar{F}_{rL}$$

$$\frac{\partial \bar{V}_I \cdot \bar{V}_L}{\partial t} = -\nabla_3 \cdot [(\bar{V}_I \cdot \bar{V}_L)\bar{V}_{3M} + \bar{V}_{3L}\Phi_I + \bar{V}_{3I}\Phi_L] - \bar{V}_L \cdot (\bar{V}_{3I} \cdot \nabla_3 \bar{V}_M) - \bar{V}_I \cdot (\bar{V}_{3L} \cdot \nabla_3 \bar{V}_M) - \bar{V}_L \cdot (\bar{V}_{3T} \cdot \nabla_3 \bar{V}_T) - \bar{V}_I \cdot (\bar{V}_{3T} \cdot \nabla_3 \bar{V}_T) + \omega_L \alpha_I + \omega_I \alpha_L + \bar{V}_L \cdot \bar{F}_{rI} + \bar{V}_I \cdot \bar{F}_{rL}$$

$$\frac{\partial \bar{V}_H \cdot \bar{V}_M}{\partial t} = -\nabla_3 \cdot [(\bar{V}_H \cdot \bar{V}_M)\bar{V}_{3M} + \bar{V}_{3M}\Phi_H + \bar{V}_{3H}\Phi_M] - \bar{V}_{3H} \cdot \nabla_3 K_M - \bar{V}_M \cdot \bar{V}_{3T} \cdot \nabla_3 \bar{V}_T - \bar{V}_H \cdot \bar{V}_{3T} \cdot \nabla_3 \bar{V}_T + \omega_M \alpha_H + \omega_H \alpha_M + \bar{V}_M \cdot \bar{F}_{rH} + \bar{V}_H \cdot \bar{F}_{rM}$$

$$\frac{\partial \bar{V}_I \cdot \bar{V}_M}{\partial t} = -\nabla_3 \cdot [(\bar{V}_I \cdot \bar{V}_M)\bar{V}_{3M} + \bar{V}_{3M}\Phi_I + \bar{V}_{3I}\Phi_M] - \bar{V}_{3I} \cdot \nabla_3 K_M - \bar{V}_M \cdot \bar{V}_{3T} \cdot \nabla_3 \bar{V}_T - \bar{V}_I \cdot \bar{V}_{3T} \cdot \nabla_3 \bar{V}_T + \omega_M \alpha_I + \omega_I \alpha_M + \bar{V}_M \cdot \bar{F}_{rI} + \bar{V}_I \cdot \bar{F}_{rM}$$

$$\frac{\partial \bar{V}_L \cdot \bar{V}_M}{\partial t} = -\nabla_3 \cdot [(\bar{V}_L \cdot \bar{V}_M)\bar{V}_{3M} + \bar{V}_{3M}\Phi_L + \bar{V}_{3L}\Phi_M] - \bar{V}_{3L} \cdot \nabla_3 K_M - \bar{V}_M \cdot \bar{V}_{3T} \cdot \nabla_3 \bar{V}_T - \bar{V}_L \cdot \bar{V}_{3T} \cdot \nabla_3 \bar{V}_T + \omega_M \alpha_L + \omega_L \alpha_M + \bar{V}_M \cdot \bar{F}_{rL} + \bar{V}_L \cdot \bar{F}_{rM}$$

The sum of the first terms on the right hand side (RHS) of the above equations gives

$$\begin{aligned} RHS1 &= -\nabla_3(\bar{V}_{3M}K_H + \bar{V}_{3H}\Phi_H) - \nabla_3(\bar{V}_{3M}K_I + \bar{V}_{3I}\Phi_I) \\ &\quad - \nabla_3(\bar{V}_{3M}K_L + \bar{V}_{3L}\Phi_L) - \nabla_3(\bar{V}_{3M}K_M + \bar{V}_{3M}\Phi_M) \\ &\quad - \nabla_3 \cdot [(\bar{V}_H \cdot \bar{V}_I)\bar{V}_{3M} + \bar{V}_{3I}\Phi_H + \bar{V}_{3H}\Phi_I] \\ &\quad - \nabla_3 \cdot [(\bar{V}_I \cdot \bar{V}_L)\bar{V}_{3M} + \bar{V}_{3L}\Phi_I + \bar{V}_{3I}\Phi_L] \\ &\quad - \nabla_3 \cdot [(\bar{V}_H \cdot \bar{V}_L)\bar{V}_{3M} + \bar{V}_{3L}\Phi_H + \bar{V}_{3H}\Phi_L] \\ &\quad - \nabla_3 \cdot [(\bar{V}_H \cdot \bar{V}_M)\bar{V}_{3M} + \bar{V}_{3M}\Phi_H + \bar{V}_{3H}\Phi_M] \\ &\quad - \nabla_3 \cdot [(\bar{V}_I \cdot \bar{V}_M)\bar{V}_{3M} + \bar{V}_{3M}\Phi_I + \bar{V}_{3I}\Phi_M] \\ &\quad - \nabla_3 \cdot [(\bar{V}_L \cdot \bar{V}_M)\bar{V}_{3M} + \bar{V}_{3M}\Phi_L + \bar{V}_{3L}\Phi_M] \\ &= -\nabla_3[\bar{V}_{3M}(K_H + K_I + K_L + K_M)] \\ &\quad - \nabla_3 \cdot [(\bar{V}_H \cdot \bar{V}_I + \bar{V}_H \cdot \bar{V}_L + \bar{V}_I \cdot \bar{V}_L + \bar{V}_H \cdot \bar{V}_M \\ &\quad + \bar{V}_I \cdot \bar{V}_M + \bar{V}_L \cdot \bar{V}_M)\bar{V}_{3M}] \\ &\quad - \nabla_3 \cdot [(\bar{V}_{3H} + \bar{V}_{3I} + \bar{V}_{3L} + \bar{V}_{3M})\Phi_H \\ &\quad + (\bar{V}_{3H} + \bar{V}_{3I} + \bar{V}_{3L} + \bar{V}_{3M})\Phi_I \\ &\quad + (\bar{V}_{3H} + \bar{V}_{3I} + \bar{V}_{3L} + \bar{V}_{3M})\Phi_L \\ &\quad + (\bar{V}_{3H} + \bar{V}_{3I} + \bar{V}_{3L} + \bar{V}_{3M})\Phi_M] \\ &= -\nabla_3\left[\frac{1}{2}\bar{V}_{3M}(\bar{V}_H \cdot \bar{V}_H + \bar{V}_I \cdot \bar{V}_I + \bar{V}_L \cdot \bar{V}_L \right. \\ &\quad \left. + \bar{V}_M \cdot \bar{V}_M + 2\bar{V}_H \cdot \bar{V}_I + 2\bar{V}_H \cdot \bar{V}_L + 2\bar{V}_I \cdot \bar{V}_L \right. \\ &\quad \left. + 2\bar{V}_H \cdot \bar{V}_M + 2\bar{V}_I \cdot \bar{V}_M + 2\bar{V}_L \cdot \bar{V}_M)\right] \\ &\quad - \nabla_3 \cdot [(\bar{V}_{3H} + \bar{V}_{3I} + \bar{V}_{3L} + \bar{V}_{3M}) \\ &\quad (\Phi_H + \Phi_I + \Phi_L + \Phi_M)] \\ &= -\nabla_3\left[\frac{1}{2}\bar{V}_{3M}(\bar{V}_H + \bar{V}_I + \bar{V}_L + \bar{V}_M) \right. \\ &\quad \left. (\bar{V}_H + \bar{V}_I + \bar{V}_L + \bar{V}_M)\right] - \nabla_3 \\ &\quad \cdot [(\bar{V}_{3H} + \bar{V}_{3I} + \bar{V}_{3L} + \bar{V}_{3M}) \\ &\quad (\Phi_H + \Phi_I + \Phi_L + \Phi_M)] \\ &= -\nabla_3\left[\frac{1}{2}\bar{V}_{3M}(\bar{V} \cdot \bar{V})\right] - \nabla_3 \cdot [\bar{V}\Phi] \end{aligned} \tag{7}$$

The sum of the baroclinic conversion terms gives

$$\begin{aligned}
 BC &= \omega_H \alpha_H + \omega_I \alpha_I + \omega_L \alpha_L + \omega_M \alpha_M \\
 &+ \omega_I \alpha_H + \omega_H \alpha_I + \omega_L \alpha_H + \omega_H \alpha_L + \omega_I \alpha_L + \omega_L \alpha_I \\
 &+ \omega_M \alpha_H + \omega_H \alpha_M + \omega_M \alpha_I + \omega_I \alpha_M + \omega_M \alpha_L + \omega_L \alpha_M \\
 &= \omega_H(\alpha_H + \alpha_I + \alpha_L + \alpha_M) + \omega_I(\alpha_H + \alpha_I + \alpha_L + \alpha_M) \\
 &+ \omega_L(\alpha_H + \alpha_I + \alpha_L + \alpha_M) + \omega_M(\alpha_H + \alpha_I + \alpha_L + \alpha_M) \\
 &= (\omega_H + \omega_I + \omega_L + \omega_M)(\alpha_H + \alpha_I + \alpha_L + \alpha_M) \\
 &= \omega \alpha
 \end{aligned}
 \tag{8}$$

The sum of the mechanical dissipate terms is,

$$\begin{aligned}
 FD &= \bar{V}_H \cdot \bar{F}_{rH} + \bar{V}_I \cdot \bar{F}_{rI} + \bar{V}_L \cdot \bar{F}_{rL} + \bar{V}_M \cdot \bar{F}_{rM} \\
 &+ \bar{V}_I \cdot \bar{F}_{rH} + \bar{V}_H \cdot \bar{F}_{rI} + \bar{V}_L \cdot \bar{F}_{rH} + \bar{V}_H \cdot \bar{F}_{rL} \\
 &+ \bar{V}_L \cdot \bar{F}_{rI} + \bar{V}_I \cdot \bar{F}_{rL} + \bar{V}_M \cdot \bar{F}_{rH} + \bar{V}_H \cdot \bar{F}_{rM} \\
 &+ \bar{V}_M \cdot \bar{F}_{rI} + \bar{V}_I \cdot \bar{F}_{rM} + \bar{V}_M \cdot \bar{F}_{rL} + \bar{V}_L \cdot \bar{F}_{rM} \\
 &= (\bar{V}_H + \bar{V}_I + \bar{V}_L + \bar{V}_M) \cdot \bar{F}_{rH} + (\bar{V}_H + \bar{V}_I + \bar{V}_L + \bar{V}_M) \cdot \bar{F}_{rI} \\
 &+ (\bar{V}_H + \bar{V}_I + \bar{V}_L + \bar{V}_M) \cdot \bar{F}_{rL} + (\bar{V}_H + \bar{V}_I + \bar{V}_L + \bar{V}_M) \cdot \bar{F}_{rM} \\
 &= (\bar{V}_H + \bar{V}_I + \bar{V}_L + \bar{V}_M) \cdot (\bar{F}_{rH} + \bar{F}_{rI} + \bar{F}_{rL} + \bar{F}_{rM}) = \bar{V} \cdot \bar{F}_r
 \end{aligned}
 \tag{9}$$

The sum of the rest of the terms is,

$$\begin{aligned}
 & - \bar{V}_H \cdot (\bar{V}_{3H} \cdot \nabla_3 \bar{V}_M) - \bar{V}_H \cdot (\bar{V}_{3T} \cdot \nabla_3 \bar{V}_T) - \bar{V}_I \cdot (\bar{V}_{3I} \cdot \nabla_3 \bar{V}_M) - \bar{V}_I \cdot (\bar{V}_{3T} \cdot \nabla_3 \bar{V}_T) - \bar{V}_L \cdot (\bar{V}_{3L} \cdot \nabla_3 \bar{V}_M) \\
 & - \bar{V}_L \cdot (\bar{V}_{3T} \cdot \nabla_3 \bar{V}_T) - \bar{V}_M \cdot (\bar{V}_{3T} \cdot \nabla_3 \bar{V}_T) - \bar{V}_I \cdot (\bar{V}_{3H} \cdot \nabla_3 \bar{V}_M) - \bar{V}_H \cdot (\bar{V}_{3I} \cdot \nabla_3 \bar{V}_M) - \bar{V}_I \cdot (\bar{V}_{3T} \cdot \nabla_3 \bar{V}_T) \\
 & - \bar{V}_H \cdot (\bar{V}_{3T} \cdot \nabla_3 \bar{V}_T) - \bar{V}_L \cdot (\bar{V}_{3H} \cdot \nabla_3 \bar{V}_M) - \bar{V}_H \cdot (\bar{V}_{3L} \cdot \nabla_3 \bar{V}_M) - \bar{V}_L \cdot (\bar{V}_{3T} \cdot \nabla_3 \bar{V}_T) - \bar{V}_H \cdot (\bar{V}_{3T} \cdot \nabla_3 \bar{V}_T) \\
 & - \bar{V}_L \cdot (\bar{V}_{3I} \cdot \nabla_3 \bar{V}_M) - \bar{V}_I \cdot (\bar{V}_{3L} \cdot \nabla_3 \bar{V}_M) - \bar{V}_L \cdot (\bar{V}_{3T} \cdot \nabla_3 \bar{V}_T) - \bar{V}_I \cdot (\bar{V}_{3T} \cdot \nabla_3 \bar{V}_T) - \bar{V}_{3H} \cdot \nabla_3 K_M - \bar{V}_M \cdot \bar{V}_{3T} \cdot \nabla_3 \bar{V}_T \\
 & - \bar{V}_H \cdot \bar{V}_{3T} \cdot \nabla_3 \bar{V}_T - \bar{V}_{3I} \cdot \nabla_3 K_M - \bar{V}_M \cdot \bar{V}_{3T} \cdot \nabla_3 \bar{V}_T - \bar{V}_I \cdot \bar{V}_{3T} \cdot \nabla_3 \bar{V}_T - \bar{V}_{3L} \cdot \nabla_3 K_M - \bar{V}_M \cdot \bar{V}_{3T} \cdot \nabla_3 \bar{V}_T - \bar{V}_L \cdot \bar{V}_{3T} \cdot \nabla_3 \bar{V}_T \\
 & = - \underbrace{\bar{V}_H \cdot \bar{V}_{3T} \cdot \nabla_3 \bar{V}_T - \bar{V}_I \cdot \bar{V}_{3T} \cdot \nabla_3 \bar{V}_T - \bar{V}_L \cdot \bar{V}_{3T} \cdot \nabla_3 \bar{V}_T - \bar{V}_M \cdot \bar{V}_{3T} \cdot \nabla_3 \bar{V}_T}_H \\
 & \quad - \underbrace{\bar{V}_H \cdot \bar{V}_{3T} \cdot \nabla_3 \bar{V}_T - \bar{V}_I \cdot \bar{V}_{3T} \cdot \nabla_3 \bar{V}_T - \bar{V}_L \cdot \bar{V}_{3T} \cdot \nabla_3 \bar{V}_T - \bar{V}_M \cdot \bar{V}_{3T} \cdot \nabla_3 \bar{V}_T}_I \\
 & \quad - \underbrace{\bar{V}_H \cdot \bar{V}_{3T} \cdot \nabla_3 \bar{V}_T - \bar{V}_I \cdot \bar{V}_{3T} \cdot \nabla_3 \bar{V}_T - \bar{V}_L \cdot \bar{V}_{3T} \cdot \nabla_3 \bar{V}_T - \bar{V}_M \cdot \bar{V}_{3T} \cdot \nabla_3 \bar{V}_T}_L \\
 & \quad - \underbrace{\bar{V}_H \cdot \bar{V}_{3T} \cdot \nabla_3 \bar{V}_T - \bar{V}_I \cdot \bar{V}_{3T} \cdot \nabla_3 \bar{V}_T - \bar{V}_L \cdot \bar{V}_{3T} \cdot \nabla_3 \bar{V}_T - \bar{V}_M \cdot \bar{V}_{3T} \cdot \nabla_3 \bar{V}_T}_M \\
 & - (\bar{V}_H + \bar{V}_I + \bar{V}_L + \bar{V}_M) \cdot (\bar{V}_{3H} \cdot \nabla_3 \bar{V}_M) - (\bar{V}_H + \bar{V}_I + \bar{V}_L + \bar{V}_M) \cdot (\bar{V}_{3I} \cdot \nabla_3 \bar{V}_M) \\
 & - (\bar{V}_H + \bar{V}_I + \bar{V}_L + \bar{V}_M) \cdot (\bar{V}_{3L} \cdot \nabla_3 \bar{V}_M) = - \bar{V} \cdot (\bar{V}_{3T} \cdot \nabla_3 \bar{V}_T) - \bar{V} \cdot (\bar{V}_{3T} \cdot \nabla_3 \bar{V}_M) \\
 & = - \bar{V} \cdot (\bar{V}_{3T} \cdot \nabla_3 \bar{V}) = - \bar{V}_{3T} \cdot \nabla_3 \left( \frac{1}{2} \bar{V} \cdot \bar{V} \right) = - \nabla_3 \left[ \frac{1}{2} \bar{V}_{3T} (\bar{V} \cdot \bar{V}) \right]
 \end{aligned}
 \tag{10}$$

Add up all the terms on the RHS of the above equations, namely (7) + (8) + (9) + (10), we have

$$\begin{aligned} RHS &= -\nabla_3 \left[ \frac{1}{2} \bar{V}_{3M} (\bar{V} \cdot \bar{V}) \right] - \nabla_3 \cdot [\bar{V}\Phi] + \omega\alpha \\ &\quad + \bar{V} \cdot \bar{F}_r - \nabla_3 \left[ \frac{1}{2} \bar{V}_{3T} (\bar{V} \cdot \bar{V}) \right] \\ &= -\nabla_3 \left[ \frac{1}{2} (\bar{V}_{3M} + \bar{V}_{3T}) (\bar{V} \cdot \bar{V}) \right] - \nabla_3 \cdot [\bar{V}\Phi] \\ &\quad + \omega\alpha + \bar{V} \cdot \bar{F}_r \\ &= -\nabla_3 \left[ \frac{1}{2} (\bar{V}_{3M} + \bar{V}_{3T}) (\bar{V} \cdot \bar{V}) + \bar{V}\Phi \right] + \omega\alpha + \bar{V} \cdot \bar{F}_r \end{aligned}$$

This recovers the total kinetic energy equation:

$$\begin{aligned} \bar{V} \cdot \frac{\partial \bar{V}}{\partial t} + \bar{V} \cdot (\bar{V} \cdot \nabla_3 \bar{V}) &= -\bar{V} \cdot \nabla \Phi - \bar{V} \cdot (f\bar{k} \times \bar{V}) + \bar{V} \cdot \bar{F}_r \\ &\Rightarrow \frac{\partial \frac{1}{2} |\bar{V}|^2}{\partial t} = -\bar{V} \cdot (\bar{V} \cdot \nabla_3 \bar{V}) - \bar{V} \cdot \nabla \Phi + \bar{V} \cdot \bar{F}_r \\ &= -\nabla_3 \left[ \frac{1}{2} (\bar{V}_{3M} + \bar{V}_{3T}) (\bar{V} \cdot \bar{V}) + \bar{V}\Phi \right] + \omega\alpha + \bar{V} \cdot \bar{F}_r \end{aligned}$$

## References

- Barriopedro D, García-Herrera R, González-Rouco J, Trigo R (2010) Application of blocking diagnosis methods to general circulation models. Part II: model simulations. *Clim Dyn* 35(7):1393–1409
- Bjerknes J (1969) Atmospheric teleconnections from the equatorial Pacific. *Mon Weather Rev* 97(3):163–172
- Black RX (1997) Deducing anomalous wave source regions during the life cycles of persistent flow anomalies. *J Atmos Sci* 54(7):895–907
- Blackmon ML, Lee YH, Wallace JM (1984a) Horizontal structure of 500 mb height fluctuations with long, intermediate and short time scales. *J Atmos Sci* 41(6):961–980
- Blackmon ML, Lee YH, Wallace JM, Hsu H-H (1984b) Time variation of 500 mb height fluctuations with long, intermediate and short time scales as deduced from lag-correlation statistics. *J Atmos Sci* 41(6):981–991
- Cai M, Mak M (1990) On the basic dynamics of regional cyclogenesis. *J Atmos Sci* 47(12):1417–1442
- Cai M, Van Den Dool HM (1994) Dynamical decomposition of low-frequency tendencies. *J Atmos Sci* 51(14):2086–2100
- Cai M, Yang S, Van Den Dool HM, Kousky VE (2007) Dynamical implications of the orientation of atmospheric eddies: a local energetics perspective. *Tellus A* 59(1):127–140
- Cash BA, Lee S (2000) Dynamical processes of block evolution. *J Atmos Sci* 57(19):3202–3218
- Chang EKM (1993) Downstream development of Baroclinic waves as inferred from regression analysis. *J Atmos Sci* 50(13):2038–2053
- Chang EKM, Lee S, Swanson KL (2002) Storm track dynamics. *J Clim* 15(16):2163–2183
- Deng Y, Jiang T (2011) Intraseasonal modulation of the North Pacific storm track by tropical convection in boreal winter. *J Clim* 24(4):1122–1137
- Deng Y, Mak M (2005) An idealized model study relevant to the dynamics of the midwinter minimum of the Pacific storm track. *J Atmos Sci* 62(4):1209–1225
- Deng Y, Mak M (2006) Nature of the differences in the intraseasonal variability of the Pacific and Atlantic storm tracks: a diagnostic study. *J Atmos Sci* 63(10):2602–2615
- Doblas-Reyes FJ, Casado MJ, Pastor MA (2002) Sensitivity of the Northern Hemisphere blocking frequency to the detection index. *J Geophys Res* 107(D2):4009
- Dole RM (2008) Linking weather and climate. *Meteorol Monogr* 33(55):297–348
- Dole RM, Black RX (1990) Life cycles of persistent anomalies. Part II: the development of persistent negative height anomalies over the North Pacific Ocean. *Mon Weather Rev* 118(4):824–846
- Dole RM, Gordon ND (1983) Persistent anomalies of the extratropical northern hemisphere wintertime circulation: geographical distribution and regional persistence characteristics. *Mon Weather Rev* 111(8):1567–1586
- Duchon CE (1979) Lanczos filtering in one and two dimensions. *J Appl Meteorol* 18(8):1016–1022
- Egger J (1978) Dynamics of blocking highs. *J Atmos Sci* 35(10):1788–1801
- Holton JR (2004) An introduction to dynamic meteorology, 4th edn. Elsevier Academic Press, Burlington, xii, 535 pp
- Hsu P-c, Li T, Tsou C-H (2010) Interactions between boreal summer intraseasonal oscillations and synoptic-scale disturbances over the Western North Pacific. Part I: energetics diagnosis. *J Clim* 24(3):927–941
- Jiang T, Deng Y (2011) Downstream modulation of North Pacific atmospheric river activity by East Asian cold surges. *Geophys Res Lett* 38(20):L20807
- Kanamitsu M, Ebisuzaki W, Woollen J, Yang S-K, Hnilo JJ, Fiorino M, Potter GL (2002) NCEP–DOE AMIP-II Reanalysis (R-2). *Bull Am Meteorol Soc* 83(11):1631–1643
- Lau N-C (1988) Variability of the observed midlatitude storm tracks in relation to low-frequency changes in the circulation pattern. *J Atmos Sci* 45(19):2718–2743
- Lorenz EN (1955) Available potential energy and the maintenance of the general circulation. *Tellus* 7(2):157–167
- Mak M (1991) Dynamics of an atmospheric blocking as deduced from its local energetics. *Q J R Meteorol Soc* 117(499):477–493
- Mak M, Cai M (1989) Local barotropic instability. *J Atmos Sci* 46(21):3289–3311
- Mak M, Deng Y (2007) Diagnostic and dynamical analyses of two outstanding aspects of storm tracks. *Dyn Atmos Oceans* 43(1–2):80–99
- Matsueda M, Mizuta R, Kusunoki S (2009) Future change in wintertime atmospheric blocking simulated using a 20-km-mesh atmospheric global circulation model. *J Geophys Res* 114(D12):D12114
- Mullen SL (1987) Transient eddy forcing of blocking flows. *J Atmos Sci* 44(1):3–22
- Nakamura H (1992) Midwinter suppression of baroclinic wave activity in the Pacific. *J Atmos Sci* 49(17):1629–1642
- Nakamura H, Wallace JM (1990) Observed changes in Baroclinic wave activity during the life cycles of low-frequency circulation anomalies. *J Atmos Sci* 47(9):1100–1116
- Nakamura H, Wallace JM (1993) Synoptic behavior of Baroclinic eddies during the blocking onset. *Mon Weather Rev* 121(7):1892–1903
- Nakamura H, Nakamura M, Anderson JL (1997) The role of high- and low-frequency dynamics in blocking formation. *Mon Weather Rev* 125(9):2074–2093
- Namias J (1947) Characteristics of the general circulation over the Northern Hemisphere during the abnormal winter 1946–47. *Mon Weather Rev* 75(8):145–152

- Oort AH (1964) On estimates of the atmospheric energy cycle. *Mon Weather Rev* 92(11):483–493
- Orlanski I, Katzfey J (1991) The life cycle of a cyclone wave in the Southern hemisphere. Part I: eddy Energy Budget. *J Atmos Sci* 48(17):1972–1998
- Peixoto JP, Oort AH (1992) *Physics of climate*, xxxix. American Institute of Physics, New York, 520 p
- Plumb RA (1983) A new look at the energy cycle. *J Atmos Sci* 40(7):1669–1688
- Reinhold B (1987) Weather regimes: the challenge in extended-range forecasting. *Science* 235(4787):437–441
- Scaife AA, Woollings T, Knight J, Martin G, Hinton T (2010) Atmospheric blocking and mean biases in climate models. *J Clim* 23(23):6143–6152
- Sheng J, Derome J (1991) An observational study of the energy transfer between the seasonal mean flow and transient eddies. *Tellus A* 43(2):128–144
- Sheng J, Hayashi Y (1990a) Estimation of atmospheric energetics in the frequency domain during the FGGE year. *J Atmos Sci* 47(10):1255–1268
- Sheng J, Hayashi Y (1990b) Observed and simulated energy cycles in the frequency domain. *J Atmos Sci* 47(10):1243–1254
- Shutts GJ (1983) The propagation of eddies in diffluent jetstreams: eddy vorticity forcing of ‘blocking’ flow fields. *Q J R Meteorol Soc* 109(462):737–761
- Shutts GJ (1986) A case study of eddy forcing during an atlantic blocking episode. *Adv Geophys* 29:135–162
- Trenberth KE (1986) An assessment of the impact of transient eddies on the zonal flow during a blocking episode using localized Eliassen-Palm Flux diagnostics. *J Atmos Sci* 43(19):2070–2087
- Trenberth KE, Hurrell JW (1994) Decadal atmosphere-ocean variations in the Pacific. *Clim Dyn* 9(6):303–319
- Trenberth KE, Branstator GW, Karoly D, Kumar A, Lau NC, Ropelewski C (1998) Progress during TOGA in understanding and modeling global teleconnections associated with tropical sea surface temperatures. *J Geophys Res* 103(C7):14291–14324
- Tyrlis E, Hoskins BJ (2008) Aspects of a northern hemisphere atmospheric blocking climatology. *J Atmos Sci* 65(5):1638–1652
- Wallace JM, Lau NC (1985) On the role of barotropic energy conversions in the general circulation. *Adv Geophys* 28A:33–74
- Wiin-Nielsen A (1962) On transformation of kinetic energy between the vertical shear flow and the vertical mean flow in the atmosphere. *Mon Weather Rev* 90(8):311–323